Journal of Magnetic Resonance **148,** 53–60 (2001)
doi:10.1006/jmre.2000.2227, available online at http://www.idealibrary.com on IDEAL®

Methods for the Measurement of $^{1}J_{NC\alpha}$ and $^{2}J_{NC\alpha}$ from a Simplified 2D $^{13}C^{\alpha}$-Coupled ^{15}N SE–HSQC Spectrum

Sami Heikkinen, Perttu Permi, and Ilkka Kilpeläinen

Institute of Biotechnology, NMR Laboratory, P.O. Box 56, FIN-00014 University of Helsinki, Finland

Received May 15, 2000; revised September 14, 2000

Two methods for the measurement of $^{2}J_{NC\alpha}$ and $^{1}J_{NC\alpha}$ in $^{15}N/^{13}C$-labeled small and medium-size proteins are described. The current approach is based on simplified $^{13}C^{\alpha}$-coupled ^{15}N HSQC spectra, where the two $^{2}J_{NC\alpha}$ doublets are separated into two subspectra corresponding to the α and β spin states of the residue's own α carbon. The displacement of the two $^{2}J_{NC\alpha}$ doublets between the two subspectra provides an accurate value for $^{1}J_{NC\alpha}$. The α/β filtration is achieved by taking the sum and difference of the recorded complementary in-phase and antiphase *J*-coupled spectra. *J*-multiplication is utilized in one of the proposed methods. In this method, an additional coupling evolution period, which is incremented in concert with t_1, is included in the pulse sequence making it possible to scale the peak-to-peak separation. © 2001 Academic Press

Key Words: **NMR; α/β filtration; IPAP method; S^{3}CT; HSQC; coupling constant; ubiquitin; *J*-multiplication; protein.**

INTRODUCTION

The determination of protein structure with NMR spectroscopy is traditionally based on the use of NOE and torsion angle constraints (*1, 2*). The torsion angles are obtained by converting the measured coupling constants (homo- or heteronuclear) over three bonds (^{3}J) into torsion angle information with Karplus equations (*3, 4*). Recently, methods that allow accurate measurement of couplings over one (^{1}J) or two bonds (^{2}J) have been presented (*5–14*). The one- and two-bond couplings can be used in structural calculations, especially when the protein is dissolved in oriented media (*15, 16*). In a weakly aligned system the observed coupling has contributions from both scalar and dipolar couplings. The residual dipolar coupling (^{1}D or ^{2}D), resulting from incomplete rotational averaging, contains unique structural information, i.e., orientation of the internuclear vector with respect to the molecular alignment tensor (*15, 16*). The residual couplings can be readily retrieved by monitoring the difference between the couplings measured from the sample in isotropic and anisotropic phases.

Since protein structure determination usually starts with sequential assignment, an assigned ^{15}N HSQC spectrum is available in the early phase of the work. Therefore, our aim has been to develop methods allowing the direct measurement of the desired couplings from the two-dimensional ^{15}N–^{1}H correlation experiments with spectra superficially resembling the normal ^{15}N HSQC spectrum, without prior knowledge of full ^{1}H or ^{13}C assignments. These methods include the measurement of $^{1}J_{HN}$, $^{1}J_{NC'}$, $^{1}J_{NC\alpha}$, $^{2}J_{HNC'}$, $^{2}J_{NC\alpha}$, $^{1}J_{C'C\alpha}$, and $^{3}J_{HNH\alpha}$, just to mention some (*14, 17–22*).

In principle, the heteronuclear coupling between the nitrogen and α-carbon of the same residue can be measured from a ^{13}C-coupled ^{15}N HSQC spectrum. Simplification of the cross-peak pattern can be achieved using carbonyl decoupling during the t_1 period. As a result, couplings only to the α-carbon of the same residue (i), as well to the α-carbon of the preceding residue ($i-1$), evolve. Thus, the correlation peak is split into four lines in the indirectly detected dimension. Now the $^{1}J_{NC\alpha}$ (9–12 Hz) and $^{2}J_{NC\alpha}$ (6–9 Hz) can be measured, provided that the linewidth in the f_1 dimension allows the separation of all four lines. In practice, however, all four lines are seldom resolved, even for small proteins, and the multiplet appears as a broad triplet. One solution to further simplify the multiplet structure is to separate two doublets originating from $^{2}J_{NC\alpha}$ into two subspectra with respect to larger $^{1}J_{NC\alpha}$. This can be accomplished by performing α/β filtration with respect to $C^{\alpha}(i)$'s spin states prior to the $^{13}C^{\alpha}$-coupled ^{15}N HSQC. The resulting two spectra, corresponding to the α and β states of $C^{\alpha(i)}$ spin, would then both contain cross peaks split by $^{2}J_{NC\alpha}$, and the displacement of $^{2}J_{NC\alpha}$ doublets in the f_1 dimension between the two subspectra would determine $^{1}J_{NC\alpha}$. Such pulse sequences, enabling the separation of the α and β states of $C^{\alpha}(i)$ prior to ^{15}N HSQC, can be constructed from the sensitivity-enhanced ^{13}C–HSQC–TOCSY–^{15}N–HSQC sequence by modifying the ^{13}C HSQC period in order to obtain the separation of the α and β states utilizing either the IPAP (*8*) or the S^{3}CT approach (*10, 23, 24*). Essentially, the key idea behind the resulting pulse sequence is quite similar to the sequences designed for the measurement of proton–heteronucleus or proton–proton coupling constants presented by Sørensen *et al.*, Xu *et al.*, and Kozminski *et al.* (*10, 11, 23, 25–27*). The pulse sequences used in this work are presented in Fig. 1.

1090-7807/01 $35.00

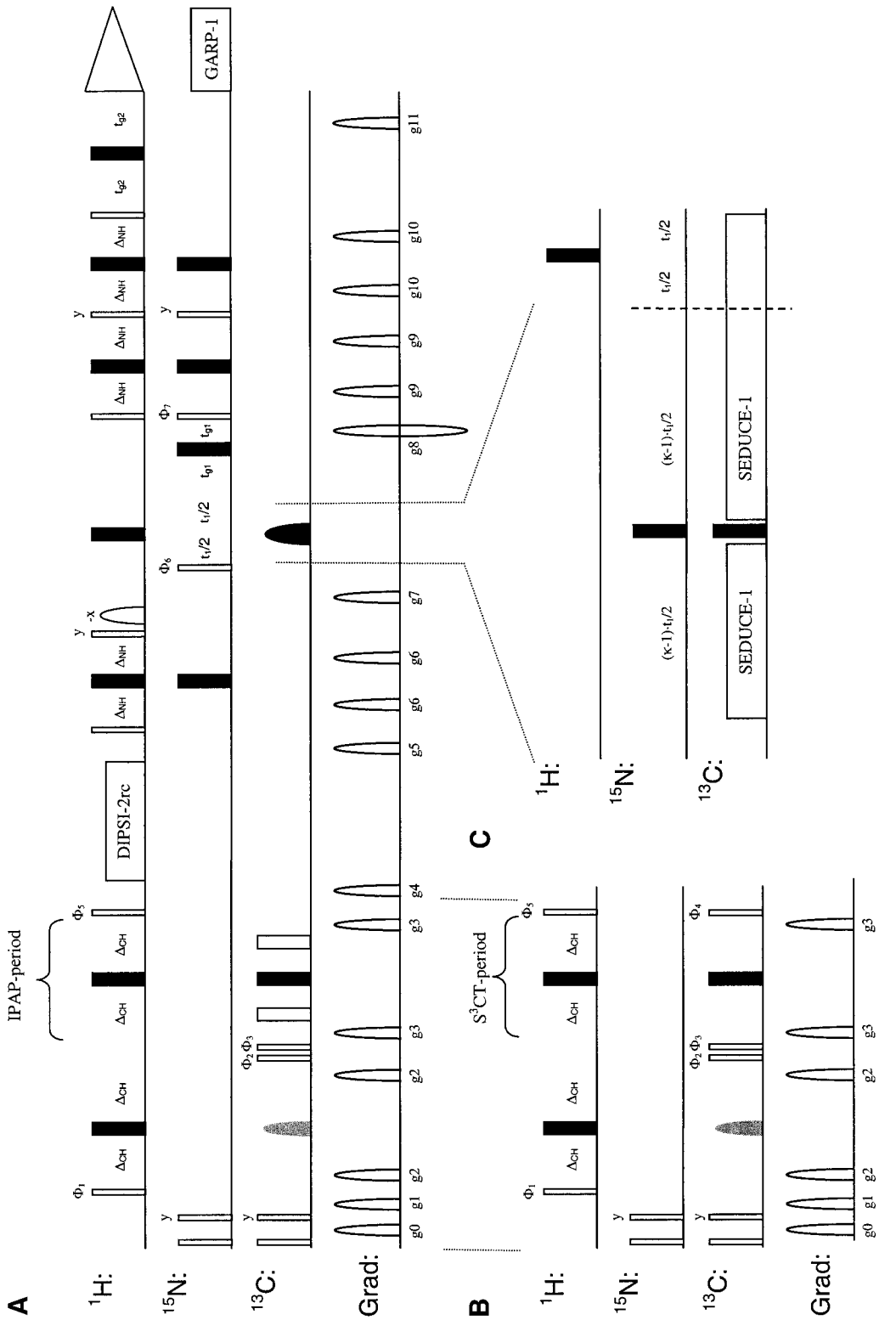
A
IPAP-period
DIPSI-2rc
GARP-1
B
S3CT-period
C
SEDUCE-1
SEDUCE-1
1H:
15N:
13C:
Grad:

DESCRIPTION OF THE PULSE SEQUENCES

All of the pulse sequences presented in Fig. 1 begin with a modified INEPT period. A band-selective 180° pulse applied at C^α frequencies is used to maximize the exclusive coherence transfer from H^α's to amide protons later in the sequence. Phase-cycling of the ^{13}C 90° pulse after the first delay 2Δ ensures that all the detectable magnetization originates from ^{13}C-bound protons and not from H^α's bound to ^{12}C due to incomplete ^{13}C enrichment. A spin-state-selective filter of length $2\Delta = \frac{1}{2}{}^1J_{CH}$ is subsequently applied utilizing either the IPAP (*8*) or the S^{3}CT approach (*10, 23, 24*) (Figs. 1A and 1B, respectively). Two separate experiments are recorded, one where the heteronuclear antiphase magnetization is refocused ("in-phase" spectrum, or IP spectrum) and an other one where it is left unperturbed ("antiphase" spectrum, or AP spectrum) prior to TOCSY mixing. During the *z*-filtered TOCSY mixing period the α-proton magnetization is transferred to the amide proton. The isotropic mixing is followed by sensitivity-enhanced, gradient-selected ^{15}N HSQC. During the t_1 period, the ^{15}N chemical shifts as well as coupling constants $^1J_{NC\alpha}$ and $^2J_{NC\alpha}$ evolve, whereas couplings to carbonyl carbons are decoupled. The resulting correlation peak in the IP spectrum is *in-phase* with respect to both $^1J_{NC\alpha}$ and $^2J_{NC\alpha}$ in the f_1 domain. Correspondingly, the correlation peak of the AP spectrum is *in-phase* with respect to $^2J_{NC\alpha}$, but *antiphase* with respect to $^1J_{NC\alpha}$. Thus, by taking the sum and difference of the two experiments, subspectra corresponding α and β states of $C^\alpha(i)$ can be constructed and $^1J_{NC\alpha}$ can be readily measured from the f_1 frequency displacement of 2D correlation peaks between the two subspectra. If ^{13}C decoupling is not applied during the acquisition, the proposed methods also allow the measurement of $^2J_{HNC\alpha(i)}$ and $^3J_{HNC\alpha(i-1)}$, provided that the resolution in the f_2 domain is sufficient. These couplings can be retrieved from an E.COSY-type tilt, i.e., frequency separation in the f_2 domain of the $^2J_{NC\alpha}$ doublet gives the value for $^3J_{HNC\alpha(i-1)}$ and f_2 separation between the two $^2J_{NC\alpha}$ doublets corresponding to the α and β states of $C^\alpha(i)$ gives the value for $^2J_{HNC\alpha(i)}$. However, since the $^2J_{NC\alpha}$ is usually relatively small, it may be tedious to measure $^3J_{HNC\alpha(i-1)}$ from the poorly resolved $^2J_{NC\alpha}$ doublet.

The advantage of the S^{3}CT method over the IPAP approach lies in the equal amount of pulses involved in recording the IP and AP spectra. This can be of importance when the ^{13}C pulses are not properly calibrated or if the RF inhomogenity of the ^{13}C coil is substantial. On the other hand, when the S^{3}CT element is used, the separation of subspectra corresponding to α and β states fails for glycine residues. Thus, when the AP spectrum is recorded, the passive heteronuclear one-bond coupling $^1J_{C\alpha H\alpha(2)}$ between C^α and the second α-proton $H^{\alpha(2)}$ of glycine evolves during the S^{3}CT period. After the S^{3}CT element, the glycine magnetization is described by the product operator $H_x^{\alpha(1)}H_z^{\alpha(2)}C_x^\alpha$, which does not allow α/β separation, whereas the corresponding product operator for non-glycine residues is $H_x^\alpha C_z^\alpha$. Due to this aforementioned drawback, we prefer the IPAP approach.

The $^2J_{NC\alpha}$'s are generally too small to be observed as well-separated in-phase doublets in the two subspectra. It is possible to circumvent this problem by modifying the pulse sequence presented in Fig. 1A (and Fig. 1B as well) with an additional evolution step for the multiplication of $^1J_{NC\alpha}$ and $^2J_{NC\alpha}$ (*17, 18, 28, 29*). The pulse sequence with the *J*-multiplication period is presented in Fig. 1C. This pulse sequence includes additional time period, $(\kappa - 1)*t_1$ (which is incremented in synchrony with t_1), during which the couplings between nitrogen and aliphatic carbons are modulated. The resulting IP and AP datasets are similar to those obtained without the multiplication; however, observed couplings $^1J_{NC\alpha}$ and $^2J_{NC\alpha}$ in the f_1 dimension are scaled up by a factor of κ. Furthermore, cross correlation between ^{15}N CSA and ^{15}N–$^{13}C^\alpha$ DD relaxation mechanisms is largely suppressed during the $(\kappa - 1)*t_1$ period. Because of an inherent broadening of the f_1 linewidths due to the additional incremented delay, this method may not

FIG. 1. The pulse sequences for the IPAP $^{13}C^{\alpha(i)}$ α/β-TOCSY ^{15}N SE–HSQC (A), S^{3}CT $^{13}C^{\alpha(i)}$ α/β-TOCSY ^{15}N SE–HSQC (B), and IPAP $^{13}C^{\alpha(i)}$ α/β-$J_{NC\alpha}$–mult-TOCSY ^{15}N SE–HSQC (C) sequence. Sequences A and C use the IPAP period as a spin-state-selective element, whereas in sequence B, a S^{3}CT period is utilized. Narrow (wide) bars correspond to 90° (180°) hard rectangular pulses. Gradient pulses are represented by narrow white half-ellipses denoted by g0–g11. The white half-ellipse on the ^{1}H channel represents the selective 90° sinc pulse on water resonance. The ^{1}H, ^{15}N, and ^{13}C carrier positions are 4.7 (water), 113.0 (center of the ^{15}N spectral region), and 56.0 ppm (center of the $^{13}C^\alpha$ region). The gray half ellipse on the ^{13}C channel indicates a band-selective pulse for inversion of C^α's, whereas the black half ellipse during the t_1 period indicates a carbonyl selective, off-resonance, one-lobe sinc 180° pulse. All the pulses have *x*-phase unless otherwise indicated. Delays: $\Delta_{CH} = \frac{1}{4}{}^1J_{CH}$, $\Delta_{NH} = \frac{1}{4}{}^1J_{NH}$, t_1 = incremented delay, t_{g1}, t_{g2}= gradient duration plus recovery delay. Decoupling of ^{15}N during the acquisition was accomplished using the GARP-1 sequence (*34*). The *J*-multiplied experiment is constructed from the sequence presented in A by replacing the t_1 period in A with the period shown in C. Carbonyl decoupling during the multiplication period and t_1 in the *J*-multiplied experiment was performed utilizing the off-resonance SEDUCE-1 decoupling field (*36*). κ (C) is the *J*-multiplication factor. The in- (IP) and antiphase (AP) datasets are obtained by applying one ^{13}C 180° pulse indicated by a black rectangle or two ^{13}C 180° pulses indicated by white rectangles included in the IPAP period (sequences A and C). For all schemes, the IP and AP data were collected in an interleaved manner and subsequently added and subtracted to separate the multiplet components into two subspectra. The phase cycle employed for sequences A and C is $\Phi_1 = 4(x), 4(-x)$, $\Phi_2 = x, -x$, $\Phi_3 = 8(x), 8(-x)$, $\Phi_5 = x$ for the IP experiment and $\Phi_5 = -y$ for the AP experiment; $\Phi_6 = 2(x), 2(-x)$, $\Phi_7 = x$, receiver = $x, 2(-x), x, -x, 2(x), -x, -x, 2(x), -x, x, 2(-x), x$. The phase cycle for sequence B is the same as for A and C except $\Phi_3 = 8(x), 8(-x)$ for the IP experiment and $\Phi_3 = 8(y), 8(-y)$ for the AP experiment, $\Phi_4 = 8(y), 8(-y)$ for the IP experiment and $\Phi_4 = 8(x), 8(-x)$ for the AP experiment, $\Phi_5 = -x$ for the IP experiment and $\Phi_5 = y$ for the AP experiment. In all experiments the N- and P-type coherences are recorded separately by inverting the sign of gradient g8 and the phase Φ_7 in synchrony. Axial peak displacement was obtained via the States–TPPI method (*37*) by inverting the phase Φ_6 and receiver on every second increment.

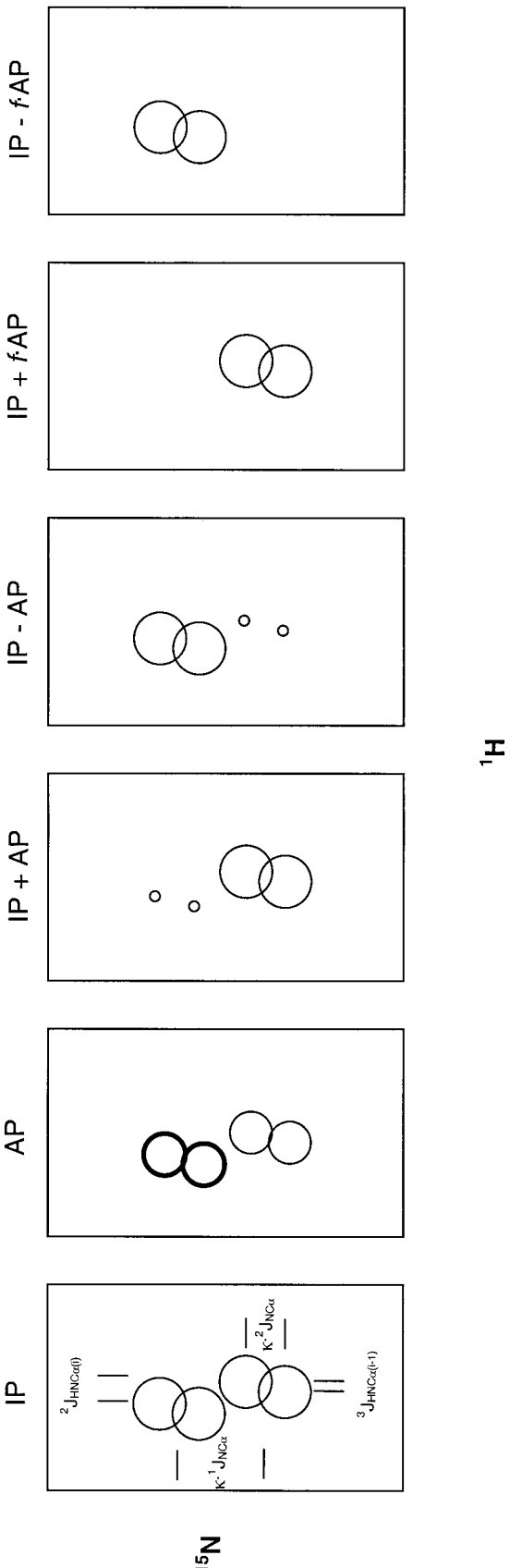

be suitable for proteins with fast ^{15}N transverse relaxation. This could be circumvented by utilizing the TROSY principle (*30*) in the highest magnetic fields. The proposed scheme could be easily modified to select the most slowly relaxing ^{15}N–^{1}H cross peak by replacing the SE–HSQC scheme with the sensitivity-enhanced, gradient-selected TROSY scheme (*31–33*). The accuracy of $^2J_{NC\alpha}$ measurement using the multiplication approach is superior to that of the nonmultiplied experiment, as $^2J_{NC\alpha}$ is measured from the peak-to-peak separation of the in-phase doublet, especially when the measured coupling is comparable to the linewidth. Therefore, in the nonmultiplied experiment this peak-to-peak separation underestimates the true $^2J_{NC\alpha}$. On the other hand, there is not such a dramatic difference between the accuracy of $^1J_{NC\alpha}$ measurements using the multiplied or nonmultiplied experiment, as this coupling is measured from the f_1 displacement of 2D correlations between the two subspectra.

Schematic 2D contour subspectra illustrating the outcome of the described experiments are shown in Fig. 2. Displacements of contours in the f_2 dimension are due to couplings $^2J_{HNC\alpha(i)}$ and $^3J_{HNC\alpha(i-1)}$ and can be removed by applying ^{13}C decoupling during the detection period. The factors κ and f correspond to the multiplication factor and the factor used in postprocessing, respectively. The AP spectrum is sketched to have lower intensity than the IP spectrum. This mimics the true situation when the proposed pulse sequences are used. After addition/subtraction of the IP and AP datasets, spin-state-selective subspectra are obtained, with the positive residual component corresponding to the undesired spin state. The origin of residual, undesired component as well as its removal is described later in the text.

In order to obtain pure subspectra associated with the α and β spin states of $C^{\alpha}(i)$, intensity imbalance between the IP and AP spectra must be minimized. Such an imbalance can arise from various sources, including the difference between the true $^1J_{C\alpha H\alpha}$ and the value used to tune the IPAP element, crosstalk originating from passive spin flips (*8, 23, 25*), TOCSY or ROESY transfer from other protons than H^{α}'s during the isotropic mixing period, and pulse imperfections, as well as imperfections in spectrometer performance. The performance of the IPAP filter was experimentally confirmed by replacing the last INEPT period of the constant-time ^{13}C HSQC (C^{α}

FIG. 2. Schematic 2D contour subspectra to illustrate the outcome of the pulse sequences presented in Fig. 1. Narrow and wide circles represent positive and negative cross peaks, respectively. In- and antiphase are marked with IP and AP, respectively. The absolute intensity of the cross peak is smaller in the AP spectrum than in the IP spectrum (see text). This results in incomplete elimination of the lines corresponding to the undesired spin state when addition/subtraction is performed to create spin-state-selective subspectra. The positive residual signals can be suppressed in postprocessing by weighting the AP spectrum with a factor $f > 1.0$ prior to addition/subtraction to create clean subspectra. The factor κ is the multiplication factor used in the pulse sequence presented in Fig. 1C.

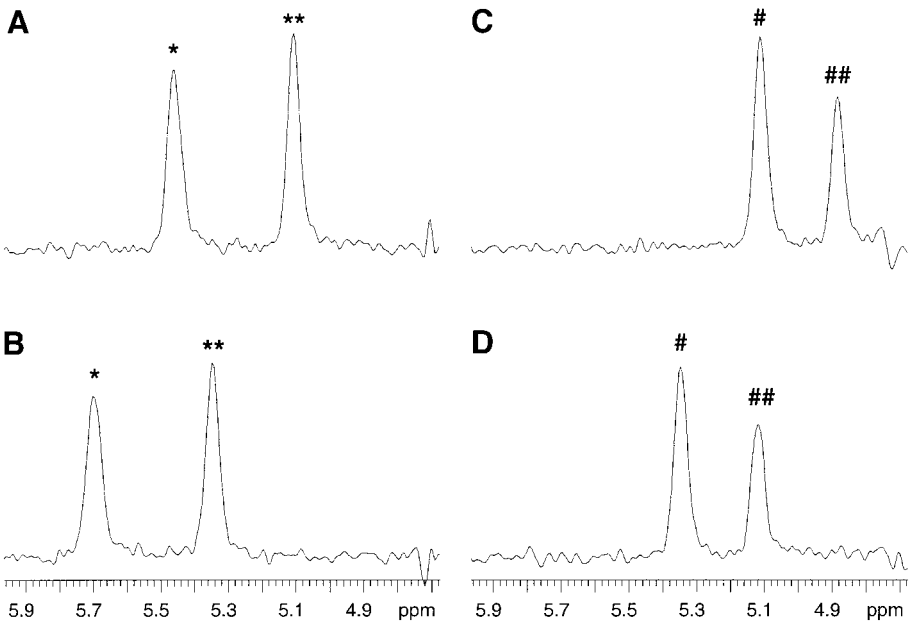

FIG. 3. 1D traces from the f_2-coupled α/β-filtered ^{13}C CT–HSQC subspectra of ^{15}N/^{13}C-labeled ubiquitin. The pulse sequence setup is described in the text. Carbon traces A,B and C,D were taken at 52.6 and 59.8 ppm, respectively. Traces A and C correspond to spin-state-selective subspectrum generated by summing the IP and AP datasets. Correspondingly, traces B and D are extracted from 2D spectrum obtained by subtracting the IP and AP datasets. Spectral lines marked with same symbol (*, **, #, ##) belong to the same proton. Pulse widths, power levels, and carrier positions are the same as described in the legend to Fig. 4. No ^{13}C decoupling was applied during the acquisition, whereas ^{15}N decoupling was accomplished using GARP-1 (*35*). The spectral width was 5497.5 (^{1}H) and 9100.0 Hz (^{13}C). The f_2-coupled α/β-filtered ^{13}C CT–HSQC experiment was acquired using 16 transients and 1024 (^{1}H) $\times$ 250 (^{13}C) points. A cosine bell apodization function was used in both dimensions and the matrix was zero filled to 4096 (^{1}H) $\times$ 1024 (^{13}C) points prior to Fourier transform. Constant-time and relaxation delays of 28 ms and 1.0 s were used, respectively.

band-selective 180° pulse was used in the first INEPT period) with the IPAP period and omitting the ^{13}C decoupling during acquisition. Two experiments were performed in an interleaved manner to record both IP and AP spectra. Thus, the addition and subtraction of these two experiments give the subspectra corresponding to ^{13}C in either the α or the β state in the f_2 dimension. Figure 3 shows traces of the f_2 coupled α/β-filtered ^{13}C CT–HSQC subspectra of the ^{15}N/^{13}C-labeled ubiquitin. Comparison of the 1D traces clearly shows that the quality of α/β filtration is excellent, as there is practically no residual line corresponding to the undesired spin state. A similar α/β filtration performance was observed for all C$^\alpha$'s. This observation agrees well with the previously shown fact that the IPAP element is very tolerant to *J*-mismatches, i.e., deviation between the the actual $^1J_{C\alpha H\alpha}$ and the value used to optimize the IPAP period (*8*). It should be noted that the crosstalk exclusively originating from the *J*-mismatch would be observed as a small residual cross peak with intensity opposite to the large cross peak corresponding to the selected spin state. As the undesired components in spectra recorded using the presented experiments have the same sign as the desired ones, the dominant intensity imbalance between the IP and AP spectra originates from other previously mentioned sources. It is quite usual that the band-selective carbon pulse also inverts other carbons than exclusively C$^\alpha$'s. This will make the TOCSY and ROESY transfers from other protons than H$^\alpha$'s possible. These magnetization transfer mechanisms will enhance the cross-peak intensity in the IP spectra since couplings between ^{15}N and other aliphatic carbons in side chains are very small. To minimize the interference from possible ROESY transfer, the DIPSI-2rc sequence (*34*) was utilized. To suppress interference originating from the TOCSY transfer, the mixing time should be set as short as possible, still ensuring a reasonable signal-to-noise ratio. This approach suppresses the ROESY transfer even further.

RESULTS AND DISCUSSION

The pulse sequences presented in Fig. 1 were tested with a 1.0 mM solution of uniformly ^{15}N/^{13}C-labeled human ubiquitin (VLI Reseach, 50 mM sodium phosphate buffer in 90% H_2O/10% D_2O at pH 5.3). Selected regions of the ubiquitin spectra recorded using the pulse sequence presented in Figs. 1A and 1C are shown in Fig. 4. The IP spectrum is shown in Fig. 4A. In principle, this spectrum is similar to the C$^\alpha$-coupled ^{15}N HSQC. The expected four-line patterns (see Fig. 2) appear as broad triplets, prohibiting the measurement of $^1J_{NC\alpha}$ and $^2J_{NC\alpha}$. The α/β-filtered spectra of the same region are presented in Figs. 4B and 4C. Now the two $^2J_{NC\alpha}$ doublets can be detected separately and thus $^2J_{NC\alpha}$ can be, in principle, measured from each spectrum. In practice, the measured couplings, $^2J_{NC\alpha}$, are biased toward too small values due to reasons discussed pre-

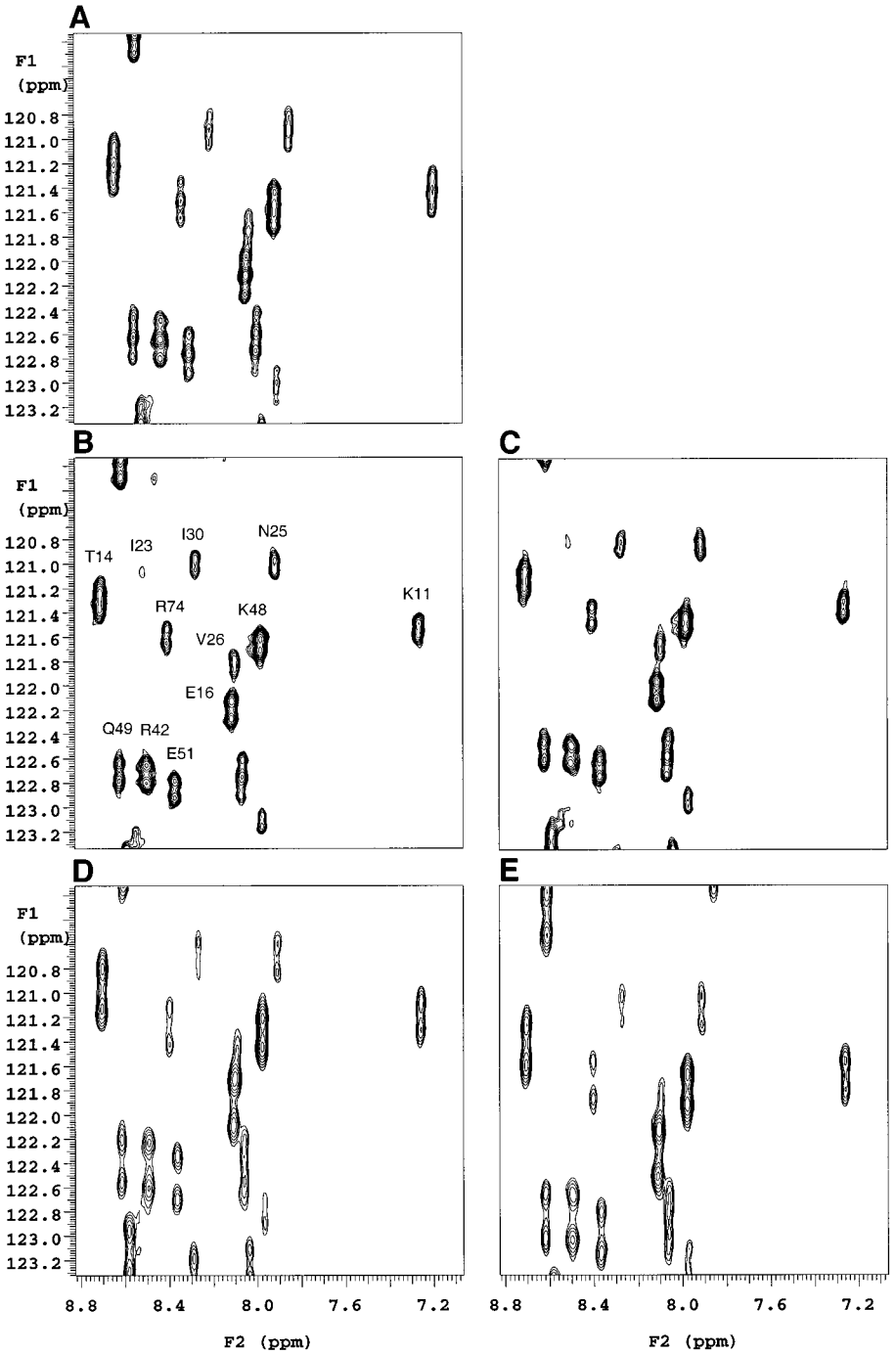

FIG. 4. Expansions of spectra recorded from 1.0 mM uniformly $^{15}N/^{13}C$-labeled ubiquitin, 90/10% H_2O/D_2O, 30°C at 600 MHz. (A) The IP spectrum was recorded using the IPAP $^{13}C^{\alpha(i)}$ α/β-TOCSY ^{15}N SE–HSQC sequence. (B) Sum and (C) difference of the IP and AP datasets from the IPAP $^{13}C^{\alpha(i)}$ α/β-TOCSY ^{15}N SE–HSQC experiment show a clear separation of the multiplet components into two subspectra according to the spin states of $C^{\alpha}(i)$. (D) Sum and (E) difference of IP and AP datasets recorded using the IPAP $^{13}C^{\alpha(i)}$ α/β-$J_{NC\alpha}$–mult-TOCSY ^{15}N SE–HSQC sequence. A multiplication factor of $\kappa = 2.5$ was used (D–E). The up- and downfield multiplet components in the multiplied experiment appear in different spectra compared to the nonmultiplied experiment. The IP and AP datasets were collected in an interleaved manner and a compensation factor of 1.20 was used to weight the AP dataset prior to addition/subtraction. The spectra were acquired using a Varian Unity INOVA 600 spectrometer. Spectral widths in both experiments were 8000 (^1H) and 2000 Hz (^{15}N). The IPAP $^{13}C^{\alpha(i)}$ α/β-TOCSY ^{15}N SE–HSQC (A–C) and the IPAP $^{13}C^{\alpha(i)}$ α/β-$J_{NC\alpha}$ mult-TOCSY ^{15}N SE–HSQC (D–E) experiments were acquired using 48 transients and 832 (^1H) × 512 (^{15}N) points and 64 transients and 832 (^1H) × 250 (^{15}N) points, respectively. A cosine bell apodization function was used in both dimensions and matrices were zero filled to 4096 (^1H) × 4096 (^{15}N) points prior to Fourier transform. Selective pulses (shape, duration, RF power): The C^{α} band-selective pulse (adiabatic sech/tanh (*38*), sweep width 30 ppm, 1.0 ms, 4.2 kHz), water-selective pulse (one-lobe sinc, 1.1 ms, 380 Hz), selective off-resonance 180° pulse on carbonyls (one-lobe sinc, 80.8 μs, 9.6 kHz), selective off-resonance carbonyl decoupling (SEDUCE-1 (*36*), 1.5 kHz). The DIPSI-2rc mixing (*34*) was applied

viously in the text. Therefore, the pulse sequence presented in Fig. 1A (and the sequence presented in Fig. 1B as well) should be used cautiously to measure values for $^2J_{NC\alpha}$. On the other hand, as $^1J_{NC\alpha}$ is measured from the frequency difference in the f_1 axis between the midpoints of $^2J_{NC\alpha}$ doublets in two α/β-filtered spectra, the accuracy of this measurement is good. Due to the intensity imbalance between the IP and AP datasets, the resulting spectra contain, in addition to the peaks of the desired spin state, residual positive signals corresponding the filtered spin state. These residual signals can be suppressed by weighting the AP spectrum by factor $f > 1.0$ prior to addition/subtraction (*23*). This procedure is schematically presented in Fig. 2. Because the TOCSY mixing time was kept short (28 ms), i.e., to minimize transfer from protons other than H^{α}'s, it could be assumed that the main source for crosstalk causing the positive residual component is passive spin flips. As this effect is dependent on local motions within the protein structure, different weighting factors may be needed for each amino acid residue in order to obtain precise values for $^1J_{NC\alpha}$ and $^2J_{NC\alpha}$. In practice, however, one or two values is sufficient (*23*). In this work we chose to use only one value ($f = 1.20$) to compensate the intensity difference, which enabled good overall suppression of the undesired component. In our hands, extending the mixing time from 28 to 47 ms resulted in the need for a compensation factor $f = 1.40$. The determination of the weighting factor by trial and error is quite straightforward if the undesired component is resolved in the f_1 domain. However, when the f_1 linewidths increase, it is more difficult to estimate the correction factor due to the broad principle component. In such a case the overall shape of the cross peak should be considered to find a proper value for the weighting factor.

The values for $^1J_{NC\alpha}$ and $^2J_{NC\alpha}$ measured from correlation peaks shown in Fig. 4 are presented in Table 1. In order to measure $^1J_{CN\alpha}$ and $^2J_{NC\alpha}$ from spectra shown in Figs. 4B–4E, the peak positions were determined using a peak-top interpolation program incorporated into standard Varian Vnmr6.1B software (except for residue I23 in spectra recorded using the sequence presented in Fig. 1A). The cross peak I23 becomes visible with the lower contour threshold. The values for $^2J_{NC\alpha}$ were measured from both sum (Table 1, $^2J_{NC\alpha(Sum)}$) and difference (Table 1, $^2J_{NC\alpha(Dif)}$) spectra obtained using the *J*-multiplied experiment and an average (Table 1, $^2J_{NC\alpha(Av)}$) was calculated. No attempts were made to measure these couplings from spectra in Figs. 4B and 4C as the in-phase doublets containing this information are not sufficiently resolved and thus the obtained values will have a bias to smaller values rather than the true coupling. The values for $^1J_{NC\alpha}$ results (Table 1, $^1J_{NC\alpha}$) obtained using both methods are in good agreement, indicating that both methods are equally suitable for measuring $^1J_{NC\alpha}$. However, in order to measure $^2J_{NC\alpha}$ reliably, the pulse sequence presented in Fig. 1C is preferred. If the correlation peak is relatively weak in the nonmultiplied experiment, the additional line broadening in the *J*-multiplied experiment can cause a significant decrease in sensitivity (Figs. 4D and 4E, residues I23, N25, and I30). It is worth mentioning that multiplication of $^2J_{NC\alpha}$ can, depending on the scaling factor, sometimes introduce overlap, which prevents the measurement of the coupling (Table 1, residues E16 and V26). It should be noted that up- and downfield multiplet components in the *J*-multiplied experiment appear in different subspectra compared to subspectra obtained without multiplication. This is due to an additional 180° ^{13}C pulse applied during the multiplication period (Fig. 1C).

The presented methods allow rapid and reliable measurement of $^2J_{NC\alpha}$, and especially $^1J_{NC\alpha}$, from ^{15}N HSQC-type spectra with simplified multiplet structures. Proposed methods enable more accurate determination of $^2J_{NC\alpha}$ and $^1J_{NC\alpha}$ than the

TABLE 1
$^1J_{NC\alpha}$ and $^2J_{NC\alpha}$ Values Measured from Spectra Shown in Fig. 4

	A	B			
Residue	$^1J_{NC\alpha}$	$^2J_{NC\alpha(Dif)}$	$^2J_{NC\alpha(Sum)}$	$^2J_{NC\alpha(Av)}$	$^1J_{NC\alpha}$
K11	11.6	5.7	5.7	5.7	11.9
T14	11.3	8.1	8.0	8.1	11.4
E16	10.2	9.4	9.3	9.4	10.2[b]
I23	12.0[a]	6.8	7.3	7.1	12.2[c]
N25	10.2	5.8	5.8	5.8	10.5
V26	9.3	—	—	—	—[d]
I30	9.9	5.1	4.4	4.8	11.3[e]
R42	10.6	9.0	9.2	9.1	10.5
K48	11.5	6.0	5.8	5.9	11.4
Q49	11.0	9.1	8.5	8.8	11.1
E51	11.2	8.7	8.4	8.6	11.2
R74	10.9	7.5	7.4	7.5	10.6

Note. Column A presents $^1J_{NC\alpha}$ values obtained using the pulse sequence illustrated in Fig. 1A. Column B contains results obtained using the *J*-multiplied experiment presented in Fig. 1C.

[a] Weak cross peaks with distorted doublet shape and peak positions were determined manually.

[b] Overlap with the cross peak of V26 in the *J*-multiplied spectra.

[c] Weak cross peaks with distorted doublet shape in the *J*-multiplied experiment.

[d] Overlap with the cross peak of E16 in the *J*-multiplied experiment; the correlation of V26 is much weaker than E16; thus no estimates for $J_{NC\alpha}$'s could be given.

[e] Distorted cross-peak shape in the *J*-multiplied experiment.

for 28 ms at an RF power of 9.3 kHz. Delays: relaxation delay = 1.0 s, $\Delta_{CH} = 1.72$ ms, $\Delta_{NH} = 2.63$ ms, $t_{g1} = 2.69$ ms, and $t_{g2} = 0.350$ ms. Gradient strengths (durations): g0 = 16.0 G/cm (0.5 ms), g1 = 11.2 G/cm (0.5 ms), g2 = 6.0 G/cm (0.5 ms), g3 = 23.0 G/cm (0.5 ms), g4 = 16.1 G/cm (0.3 ms), g5 = 13.8 G/cm (0.25 ms), g6 = 16.0 G/cm (1.0 ms), g7 = 22 G/cm (1.0 ms), g8 = 26 G/cm (2.5 ms), g9 = 4 G/cm (0.5 ms), g10 = 6.0 G/cm (0.5 ms), g11 = 26.0 G/cm (0.25 ms). All of the gradients were block shaped. ^{15}N-decoupling during acquisition was achieved using GARP-1 (*35*).

classic method, in which the coupling constants are retrieved from the multiplets in the resolution-enhanced f_1 domain of the C^{α}-coupled ^{15}N HSQC. The quite recently introduced spin-state-selective method (*14*) enabled the measurement of $^{1}J_{NC\alpha}$ and $^{2}J_{NC\alpha}$ with improved accuracy. With this aforementioned method, better accuracy is obtained for $^{2}J_{NC\alpha}$ than for $^{1}J_{NC\alpha}$, as the latter is measured from peak-to-peak separation of the in-phase doublet. In this respect, better accuracy could be obtained for $^{1}J_{NC\alpha}$ using the current methods if the linewidth in the ^{15}N dimension prevents a proper separation of the $^{1}J_{NC\alpha}$ doublet components, since the currently proposed methods allow this coupling to be measured from the cross-peak displacement in the f_1 domain between the two spin-state-selective subspectra. Since the current methods rely on editing with respect to the ^{1}H–^{13}C spin pair, they are not suitable for perdeuterated samples. Transfer via TOCSY is also more efficient for H^{α}–H^{N} moiety residing in α-helical regions of protein than for the protons in β-sheet substructures due to the difference in $^{3}J_{HNH\alpha}$. Measurement of inherently small $^{2}J_{NC\alpha}$ in larger proteins with large linewidths will be tedious with the presented methods, as the information is extracted from the peak-to-peak separation of the in-phase doublet. The measurement of $^{1}J_{NC\alpha}$ will still be possible and accurate as the $^{1}J_{NC\alpha}$ doublet components are separated according to the spin state of C^{α} in two separate spectra.

ACKNOWLEDGMENTS

This work was supported by the Academy of Finland. Professor O. W. Sørensen and Dr. A. Meissner are acknowledged for providing the pulse sequence code for the S^3CT element.

REFERENCES

1. K. Wüthrich, "NMR of Proteins and Nucleic Acids," Wiley, New York, 1986.
2. J. Cavanagh, W. J. Fairbrother, A. G. Palmer, and N. J. Skelton, "Protein NMR Spectroscopy: Principles and Practice," Academic Press, San Diego, 1996.
3. M. Karplus, *J. Chem. Phys.* **30,** 11–15, 1959.
4. V. F. Bystrov, *Prog. NMR Spectrosc.* **11,** 41–81, 1976.
5. J. R. Tolman and J. H. Prestegard, *J. Magn. Reson. B* **112,** 245–252, 1996.
6. J. R. Tolman and J. H. Prestegard, *J. Magn. Reson. B* **112,** 269–274, 1996.
7. P. Anderson, A. Annila, and G. Otting, *J. Magn. Reson.* **133,** 364–367, 1998.
8. M. Ottiger, F. Delaglio, and A. Bax, *J. Magn. Reson.* **131,** 373–378, 1998.
9. P. Anderson, K. Nordstrand, M. Sunnerhagen, E. Liepinsh, I. Turovskis, and G. Otting, *J. Biomol. NMR* **11,** 445–450, 1998.
10. A. Meissner, J. Ø. Duus, and O. W. Sørensen, *J. Biomol. NMR* **10,** 89–94, 1997.
11. A. Meissner, J. Ø. Duus, and O. W. Sørensen, *J. Magn. Reson.* **128,** 92–97, 1997.
12. M. Ottiger and A. Bax, *J. Am. Chem. Soc.* **120,** 12334–12341, 1998.
13. N. Tjandra, S. Grzesiek, and A. Bax, *J. Am. Chem. Soc.* **118,** 6264–6272, 1996.
14. P. Permi and A. Annila, *J. Biomol. NMR* **16,** 221–227 (2000).
15. N. Tjandra and A. Bax, *Science* **278,** 1111–1114, 1997.
16. A. Bax and N. Tjandra, *J. Biomol. NMR* **10,** 289–292, 1997.
17. S. Heikkinen, H. Aitio, P. Permi, R. Folmer, K. Lappalainen, and I. Kilpeläinen, *J. Magn. Reson.* **137,** 243–246, 1999.
18. P. Permi, I. Kilpeläinen, and S. Heikkinen, *Magn. Reson. Chem.* **37,** 821–826, 1999.
19. P. Permi, I. Kilpeläinen, A. Annila, and S. Heikkinen, *J. Biomol. NMR* **16,** 29–37, 2000.
20. H. Aitio and P. Permi, *J. Magn. Reson.* **143,** 391–396, 2000.
21. P. Permi, S. Heikkinen, I. Kilpeläinen, and A. Annila, *J. Magn. Reson.* **140,** 32–40, 1999.
22. P. Permi, T. Sorsa, I. Kilpeläinen, and A. Annila, *J. Magn. Reson.* **141,** 44–51, 1999.
23. M. D. Sørensen, A. Meissner, and O. W. Sørensen, *J. Magn. Reson.* **137,** 237–242, 1999.
24. A. Meissner and O. W. Sørensen, *J. Magn. Reson.* **140,** 499–503, 1999.
25. A. Meissner, T. Schulte-Herbrüggen, and O. W. Sørensen, *J. Am. Chem. Soc.* **120,** 7989–7990, 1998.
26. G. Xu, B. Zhang, and J. S. Evans, *J. Magn. Reson.* **138,** 127–134, 1999.
27. W. Kozminski, *J. Magn. Reson.* **137,** 408–412, 1999.
28. V. V. Krishnamurty, *J. Magn. Reson. B* **113,** 46–52, 1996.
29. V. V. Krishnamurty, *J. Magn. Reson. A* **121,** 33–41, 1996.
30. K. Pervushin, R. Riek, G. Wider, and K. Wüthrich, *Proc. Natl. Acad. Sci. USA* **94,** 12366–12371, 1997.
31. J. Weigelt, *J. Am. Chem. Soc.* **120,** 10778–10779, 1998.
32. M. H. Lerche, A. Meissner, F. M. Poulsen, and O. W. Sørensen, *J. Magn. Reson.* **140,** 259–263, 1999.
33. T. Schulte-Herbrüggen and O. W. Sørensen, *J. Magn. Reson.* **144,** 123–128 (2000.
34. J. Cavanagh and M. Rance, *J. Magn. Reson.* **96,** 670–678, 1992.
35. A. J. Shaka, P. B. Barker, amd R. Freeman, *J. Magn. Reson.* **64,** 547–552, 1985.
36. M. A. McCoy and L. Mueller, *J. Am. Chem. Soc.* **114,** 2108–2110, 1992.
37. D. Marion, M. Ikura, R. Tschudin, and A. Bax, *J. Magn. Reson.* **39,** 163–168, 1989.
38. M. R. Bendall, *J. Magn. Reson. A* **116,** 46–58, 1995.